

Article

Exploring the Heterocatalytic Proficiencies of ZnO Nanostructures in the Simultaneous Photo-Degradation of Chlorophenols

Ali Dad Chandio ^{1,*}, Abdul Hameed Pato ², Iftikhar Ahmed Channa ¹, Sadaf Jamal Gilani ³,
Aqeel Ahmed Shah ¹, Jaweria Ashfaq ¹, Jamil A. Buledi ², Imran Ali Chandio ⁴ and May Nasser Bin Jumah ^{5,6,7}

¹ Department of Metallurgical Engineering, NED University of Engineering and Technology, Karachi 75270, Pakistan

² National Centre of Excellence in Analytical Chemistry, University of Sindh, Jamshoro 76080, Pakistan

³ Department of Basic Health Sciences, Preparatory Year, Princess Nourah Bint Abdulrahman University, Riyadh 11671, Saudi Arabia

⁴ Institute of Chemistry, Shah Abdul Latif University, Khairpur Mirs 66111, Pakistan

⁵ Biology Department, College of Science, Princess Nourah Bint Abdulrahman University, Riyadh 11671, Saudi Arabia

⁶ Environment and Biomaterial Unit, Health Sciences Research Center, Princess Nourah Bint Abdulrahman University, Riyadh 11671, Saudi Arabia

⁷ Saudi Society for Applied Science, Princess Nourah Bint Abdulrahman University, Riyadh 11671, Saudi Arabia

* Correspondence: alidad@neduet.edu.pk



check for updates

Citation: Chandio, A.D.; Pato, A.H.; Channa, I.A.; Gilani, S.J.; Shah, A.A.; Ashfaq, J.; Buledi, J.A.; Chandio, I.A.; Jumah, M.N.B. Exploring the Heterocatalytic Proficiencies of ZnO Nanostructures in the Simultaneous Photo-Degradation of Chlorophenols. *Sustainability* **2022**, *14*, 14562. <https://doi.org/10.3390/su142114562>

Academic Editor: Zhongbing Chen

Received: 12 October 2022

Accepted: 31 October 2022

Published: 5 November 2022

Publisher's Note: MDPI stays neutral with regard to jurisdictional claims in published maps and institutional affiliations.

Abstract: The development of innovative technology for effective pollutant degradation is becoming more important as a result of major environmental issues. Here, ZnO nanoparticles were synthesized using facile and aqueous chemical growth routes. Analytical techniques such as scanning electron micrographs (SEM), energy dispersive spectroscopy (EDS), X-ray diffraction (XRD), Fourier transform infrared spectroscopy (FTIR), Zeta Seizer (ZS), and Zeta Potential were used to analyze the resultant nanoparticles (ZP). The ZnO reveals a nanocluster texture that has a medium scale of 27 nm and a surface charge (17 ± 3 mV) with a wurtzite phase and crystalline nature. Photo catalysts have a higher potential for the thermal disposal of chlorophenols pollutants due to their low cost and simple synthesis procedure. The as-prepared sample underwent photocatalysis for the simultaneous photo-degradation of PCP and TCP as a model dye under sunlight. The ZnO nanostructure exhibited an exceptional degradation of around 85–90% for PCP and TCP in the aqua liquid, with the lowest amount of catalyst dosage of 240–250 μg individually and simultaneously, over 3 min beneath the sun ray. The greater productivity of the ZnO nanostructure for natural deterioration during solar irradiation indicates that the aqueous chemical growth enables the creation of effective and affordable photocatalysts for the photodegradation of a variety of environmental contaminants.

Keywords: ZnO nanostructure; heterogeneous kinetics; aqueous chemical growth method; photocatalytic degradation; pentachlorophenol (PCP); trichlorophenol (TCP)



Copyright: © 2022 by the authors. Licensee MDPI, Basel, Switzerland. This article is an open access article distributed under the terms and conditions of the Creative Commons Attribution (CC BY) license (<https://creativecommons.org/licenses/by/4.0/>).

1. Introduction

Currently, environmental contamination is a major concern in developed and developing nations throughout the world as a result of rapid industrialization, which has resulted in an increasing degree of water pollution [1–4]. The presence of multiple chlorinated organic chemicals in the environment causes water pollution. Chlorophenols (CPs), which are widely used in the chemical, forestry, woodworking, and agricultural industries, are the most significant environmental pollutants that causes water pollution [5,6]. They are often used in the production of chemical intermediates, wood preservatives, herbicides, insecticides, and fungicides. Several CPs are mostly released into the aqueous system

without sufficient treatment, resulting in several negative environmental impacts [7]. Pentachlorophenol (PCP) and trichlorophenol (TCP) are common chlorophenols utilized in a variety of applications [8]. The majority of CPs are poisonous, mutagenic, and carcinogenic. They have the potential to create major issues, including the death of animals as well as plants. Hence, the TCP and PCP permissible limits in water are less than 10^{-4} mg/L [6,9,10]. As a result, it is critical to develop novel and effective techniques to minimize the damage caused by chlorinated organics such as CPs. PCP and TCP have been identified as important toxins in wastewater by the United States Environmental Protection Agency (US-EPA) [11,12]. As a result, there is an urgent need for the treatment of wastewater effluents, which must be cleaned to safeguard and remediate aquatic mediums for humans from lethal poisons [13–15].

Nanomaterials have recently received a lot of interest because they have good surface area–volume ratios and multiple uses in various industries, as sensors, catalysts, medicine, biotechnology, nanofertilizers, and energy storage, and are efficiently employed in drug administration. Various forms of nanomaterial shapes, such as nanorods, nanowires, nanoflakes, nanoneedles, and nanotubes, are used in photocatalytic applications [16,17]. The improved surface area–volume ratios and susceptibility are primarily responsible for the innovative and remarkable characteristics [18]. The attainment of precision, variety, durability, and restoration occur on the nanoscale. The combining of the dual advantages of binary and ternary catalysis and nanomaterials has found widespread usage in the catalytic sector. The tremendous capability of semiconductor-based photocatalysis for resolving environmental pollution challenges has been extensively acknowledged during the last few decades [19]. Among the different heterogeneous photocatalyst nanomaterials, due to their low price, zinc oxides also draw the attention of researchers, given their harmless nature and similar small band energy gap (3.37 eV) [20]. Due to its catalysis, electrical, photonic, and photon emission properties, it has a wide variety of uses. ZnO nanostructures offer a considerable advantage in catalysis reaction processes due to their large surface area and great reaction conditions [21]. Zinc oxide nanoparticles have unique strong catalyst qualities, making them an attractive choice for use, while being efficient photocatalysts for the removal of organic pollutants from the environment [22,23]. ZnO nanowires generated by the aqueous chemical growth (ACG) technique exhibit good characteristics. ACG techniques are thought to offer several benefits over others in large-scale production, including cost-efficiency, low environmental impact, and substrate compatibility. By fine-tuning the reaction and the development process, it is easy to control crucial features, including location, density, and anisotropic crystallographic orientation [24,25]. In the ACG process, ZnO is used via several approaches, including adsorption, electrochemical oxidation, catalytic wet reduction, and nanofiltration, which have been used to remove poisons from the environments [26,27]. A. Zyoud et al. [28] used a ZnO/Clay composite in the photodegradation of aqueous 2-chlorophenols (2-CP) with direct solar radiation. Without suffering a considerable decrease in efficiency, the ZnO/Clay can be efficiently used to remove CPs. After a certain time, it has been determined that the 2-CP will have fully mineralized (2 h). Nonetheless, due to the presence of chlorine and the presence of a stable aromatic ring, most conventional methods, such as innovative redox reactions, ultrafiltration, clotting cascade, electrochemical treatment, radiation treatment, electromagnetic dynamics, and photocatalytic degradation, are not suitable for the remediation of both chlorinated compounds from the environment [16,29]. Furthermore, these conventional technologies are time-consuming, require sample preparation, and are quite expensive. Among the alternatives, nanomaterial-based photocatalysis is more dependable, cost-effective, simple, reusable, and adaptable to new technologies [30–32].

In this study, a simple synthetic technique is used to create ZnO nanostructures using an aqueous chemical growth profile. To help, ZnO nanostructures are being used for the first time to degrade harmful PCP and TCP from aquatic environments simultaneously and individually. The new approach is extremely cost-effective, safe for the environment, and has outstanding anti-chlorinated phenolic compound capabilities. The nanostructure

demonstrated here is more useful and practical than the previously disclosed techniques, which offer a potential commercial standard.

2. Experimental Section

2.1. Chemical and Reagents

All of the materials and solutions used in the experimental investigation were analytical grade and pure. The precursor salt, zinc acetate, was obtained from Sigma-Aldrich Germany; NaOH (99%) was applied as a reducing agent; sodium borohydride (CAS #16940-66-2) from Sigma-Aldrich Germany was used as a proton source. From Merck Germany, Pentachloro phenol and Trichloro phenol were purchased. The entire glassware used in the experiment was completely cleaned with distilled water, then rinsed with deionized water to get the pollution off. The glassware was soaked overnight in a solution of 10% nitric acid to eliminate the residual contaminants and washed with purified water before being used in the experiment. The glassware was placed for 20 min in an oven to make it moisture-free.

2.2. Fabrication of Zinc Oxide Nanostructures

NaOH served as an alkaline solution throughout the aqueous chemical growth process used to create the zinc oxide nanostructures. In the standard procedure, a 200 mL beaker of deionized water was used to create a 0.1 M mixture of the catalyst salt zinc acetate. Similarly, a 200 mL beaker of 0.1 M NaOH solution was made in deionized water and introduced to the beaker holding the zinc acetate solution. The solution was thoroughly homogenized after the appropriate mixing and swirled for 1 h at ambient temperature. For at least 240 min, the solution was placed in an oven set at 194 °F with aluminum foil covering it. To get rid of the contaminants, the precipitates were rinsed numerous times with deionized water. The finished ZnO nanostructures were next cleaned, dried in the oven, and then annealed for four hours at 500 °C. In conclusion, the white ZnO precipitates that were produced were saved for further characterization and used to accelerate the deterioration of chlorophenols.

2.3. Heterogeneous Catalytic Measurements

The ZnO nanostructure's heterogeneous catalytic activity was tested in PCP and TCP solutions as modal pollutants. To achieve chemical equilibrium in this experiment, <15 mL of chlorinated phenol compounds with a 0.01 molar solution and 0.005 mol/L of NaBH₄ were added to a glass vial and stirred for 120 s. The nanocatalyst, PCP, and TCP were then synthesized along with the nanocatalyst. While this was going on, <5 mL of the precursor solution was used, and the UV-Vis absorption spectra for CP were noted at the wavelength 200–230 nm. Additionally, comparable processes were applied to the other parameters, including the sunlight effect, catalyst dosage, and the effect of the volume of the agent. The change in PCP and TCP absorption profiles (@220 nm) during the experimental investigation was used to calculate the percentage decrease.

$$\% \text{ Degradation} = X_i - \frac{X_f}{X_i} \times 100 \quad (1)$$

whereas X_i and X_f are the initial and final absorbances of contaminants, respectively.

2.4. Characterization Techniques

The efficacious fabrication of ZnO nanostructure was confirmed by subjecting the prepared material to various characterization tactics. An FT-IR (Thermo Nicolet 5700) study was exploited to examine the functionality of the synthesized material using a deuterated triglycine sulfate detector in the range of 4000–500 cm^{-1} at 4 cm^{-1} resolution. The crystalline nature and phase purity of ZnO nanostructures were investigated using an X-ray diffraction model (XRD-7000 Shimadzu). The elemental composition and topography of the ZnO nanostructure were examined using advanced tools such as a scanning electron micro-

scope coupled EDS model (SEM J SM 7800F). Moreover, surface potential and nanometric size distribution were explored with the help of the Zeta Seizer (Ver. 7.11 MALVAREN).

3. Results and Discussion

3.1. Characterization of Prepared Zinc Oxide Nanostructures

3.1.1. Crystalline Nature, Size, and Phase Purity Analysis ZnO Nanostructures

ZnO nanoparticles' structural consideration, elemental composition, and phase purification as prepared were examined via the X-ray diffractometric technique. The X-ray crystallographic features of synthesized zinc oxide nanostructures are displayed in Figure 1. All the characteristic diffraction patterns describe the crystallographic planes at (100) and (002), while the other supported patterns at (101), (102), (110), (103), (200), (201), (112), (004) and (202) represent the pure phase and high crystallinity of the ZnO nanostructures [33,34]. Furthermore, Figure 1 shows that the ZnO diffraction patterns were hexagonal (wurtzite), which is identical to the reported structure (JCPDS No. 36–1451). The positions and strengths of the diffraction peaks match between them. As a result, the synthesis of ZnO in a hexagonal wurtzite form was confirmed [35]. Additionally, all these patterns are referred to as ZnO nanostructures with no indication of other impurities. Using the Debye–Scherrer Equation (2), the average size distribution of ZnO nanostructures was determined.

$$D = \frac{k\lambda}{\beta \cos \theta} \quad (2)$$

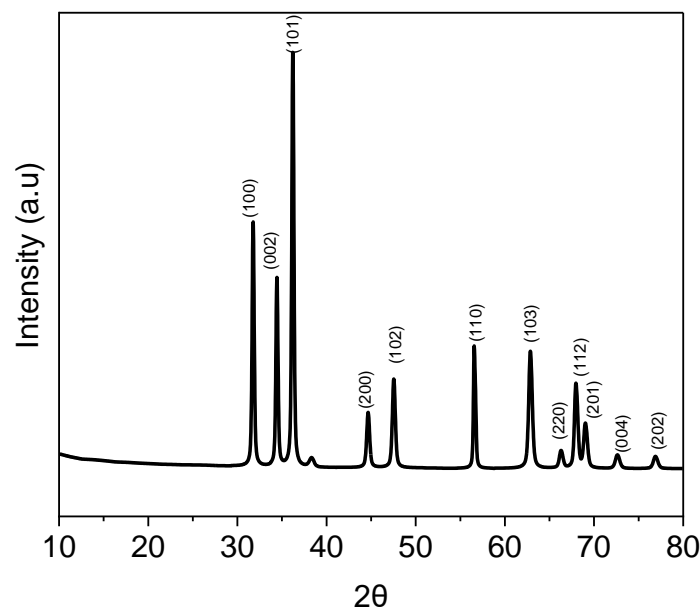


Figure 1. XRD spectra of ZnO nanostructured particles synthesized using the aqueous chemical growth method.

Equation (2) is referred as Bragg's angle, where D is the crystallite's dimensions in nanometers, k is the Scherrer constant (0.9) relating to the crystallite shape, β is the whole diameter at higher angles of the absorption edge, and is the frequency of the radiation. It was demonstrated beyond a reasonable doubt that the ZnO nanoparticles produced are crystalline in nature. This is also supported by the functional peaks in the XRD data. Furthermore, the crystalline sizes of 18 nm are calculated for the synthesized particles, and the result is in perfect agreement with the (101) peak. This peak has a size range of less than 60 nm as determined by the FWHM. The ACG has better crystallinity than those synthesized through the low-temperature hydrothermal method. It has been demonstrated that the ZnO crystallite size grows with higher annealing temperatures, and that annealing induces stress and enhanced crystallinity, while lowering lattice strain and dislocation

density through the ACG process [36,37]. The excellent crystallinity and outstanding purity of the ZnO nanostructures may provide strong catalytic activity [38].

3.1.2. Surface Morphology and Elemental Analysis of ZnO Nanostructures

The surface morphology of the ZnO nanostructure was examined using the advanced characterization tool scanning electron microscope (SEM), as indicated in Figure 2A (10,000 \times resolution) and Figure 2B (12,000 \times resolution). According to the latest research, ZnO NPs are rod forms and conglomerations of nanocrystallites. The SEM was exploited to measure the morphology and roughness of engineered nanostructures. Figure 2A,B clearly show elongated particles with rod-like nanostructure and highly porous surfaces, which makes them a suitable candidate for catalytic reactions [39]. Moreover, to examine the elemental compositions and high purities of the engineered material, SEM coupled with EDX analysis was employed as displayed in Figure 2C. The EDX spectra provide evidence that zinc and oxygen atoms are present in high elemental percentages, respectively. No other element impurity is present in the EDX spectrum, which reveals the high purity of the as-prepared material [40].

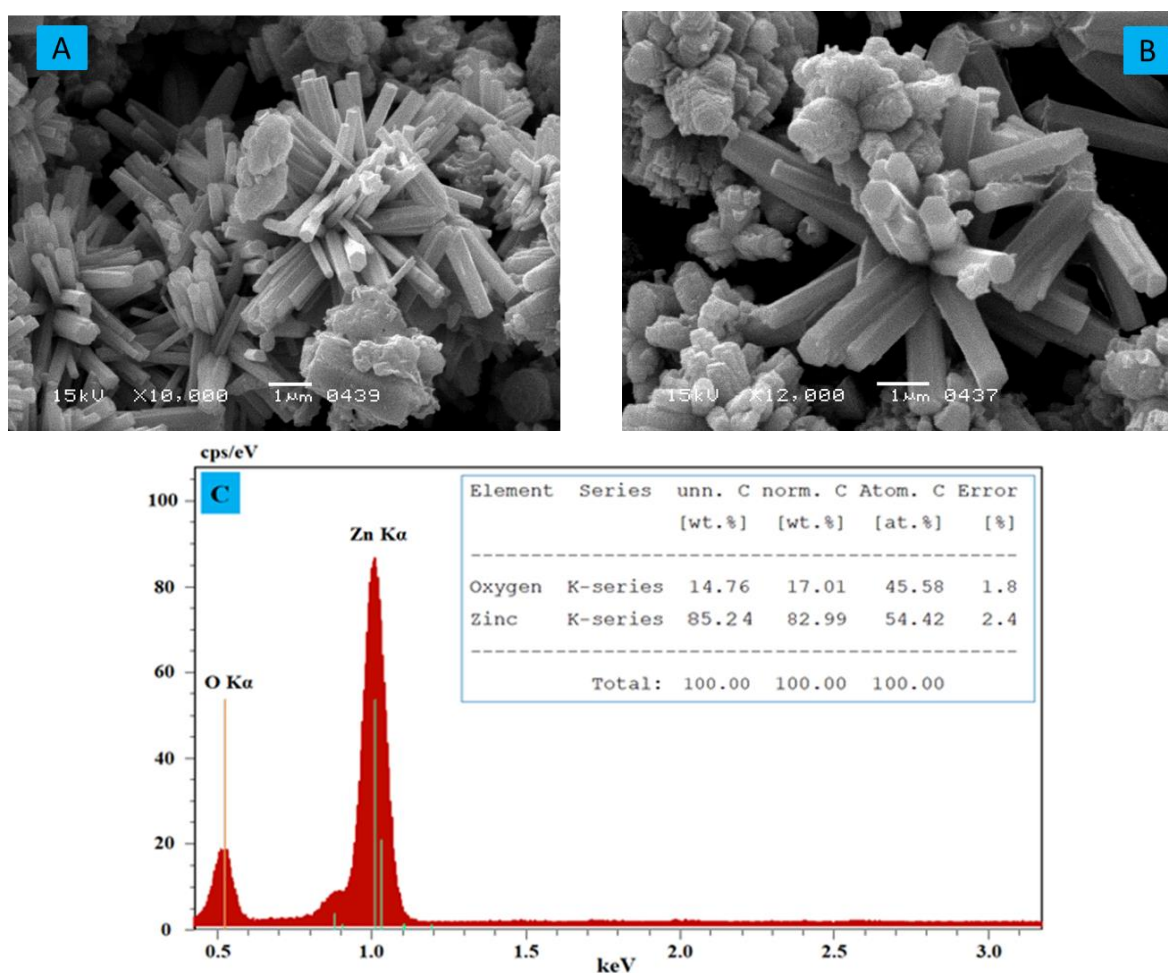


Figure 2. SEM micrographs and EDS spectra of ZnO nanoparticles, (A) SEM image of ZnO particles at 10,000 \times resolution, (B) SEM image at 12,000 \times resolution, and (C) indicates EDS spectra and the inset demonstrates the EDS results.

3.1.3. Functional Group Analysis of ZnO Nanostructures

FT-IR research was performed on the synthesis of zinc nanoparticles to discover the numerous distinctive functional groups associated with the generated nanoparticles (shown in Figure 3). The peaks represent the functional groups contained in the produced zinc

oxide nanoparticles. The main absorption peaks were found in the lower wavenumber range. The O–H stretching mode of hydroxyl groups is represented by the broadband at 3400 cm^{-1} . In the protein amide links, the highest intensity at 1634 cm^{-1} revealed amine (–NH) vibration stretching. Alcohols, phenolic groups, and C–N stretching vibrations of aromatic amines in biomolecules were reflected by the strong bands found at 1385 cm^{-1} . The Zn–O stretching bond is represented by a distinct band at 830 cm^{-1} [41]. The FTIR spectra confirm effective biomolecule capping on the NP surface, ensuring ZnO-NP stability and dispersion in aqueous conditions [42].

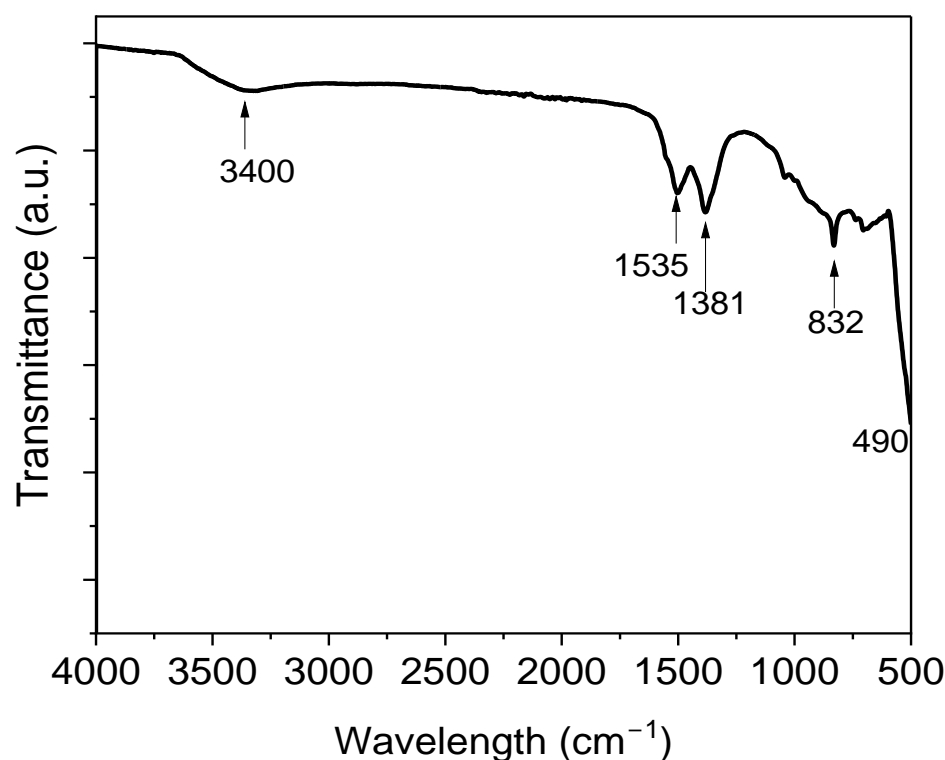


Figure 3. Fourier transform infrared spectrum of prepared ZnO nanostructured particles.

3.1.4. Surface Charge, Stability, and Nanometric Size Measurement of Prepared ZnO Nanostructures

The nanoparticles may be efficiently generated for photocatalysis, and we can effectively modify their characteristics at the nanoscale [43]. Substances have improved textures at the nanoscale, which may be large enough for the processes required. Zeta seizer analysis was carried out in this instance to assess the conductivity, durability, and nanometric dimensions. The reliability of the nanoparticle was estimated using zeta potential analysis utilizing the surface charge of the produced nanomaterials. The durability of nanomaterials in the solution is inversely correlated with the zeta potential. Figure 4B clearly illustrates the surface charge of a nanomaterial, which is around 17 mV and serves as a wonderful indicator of the photocatalysts' improved efficacy in the destruction of various pollutants. Interface energy, though, could also be used to determine the durability of nanomaterials. The particles at about 30 mV are thought to be quite stable. The created zinc oxide nanomaterials are resistant to coagulation, since 17 mV is sufficient to prevent coalescence [26]. Additionally, Figure 4 shows the produced substance's dimension A. The given image may be used to calculate the average nanometric size, which was found to be 27 nm, as shown in Figure 4A, illustrating the non-uniformity of ZnO nanoparticles produced. In comparison to particles with a wider size range, smaller particles have a larger surface area, which leads to optimum therapy delivery [44]. The exceptional performance of nanomaterials was overall proof of their small size and high surface potential [38].

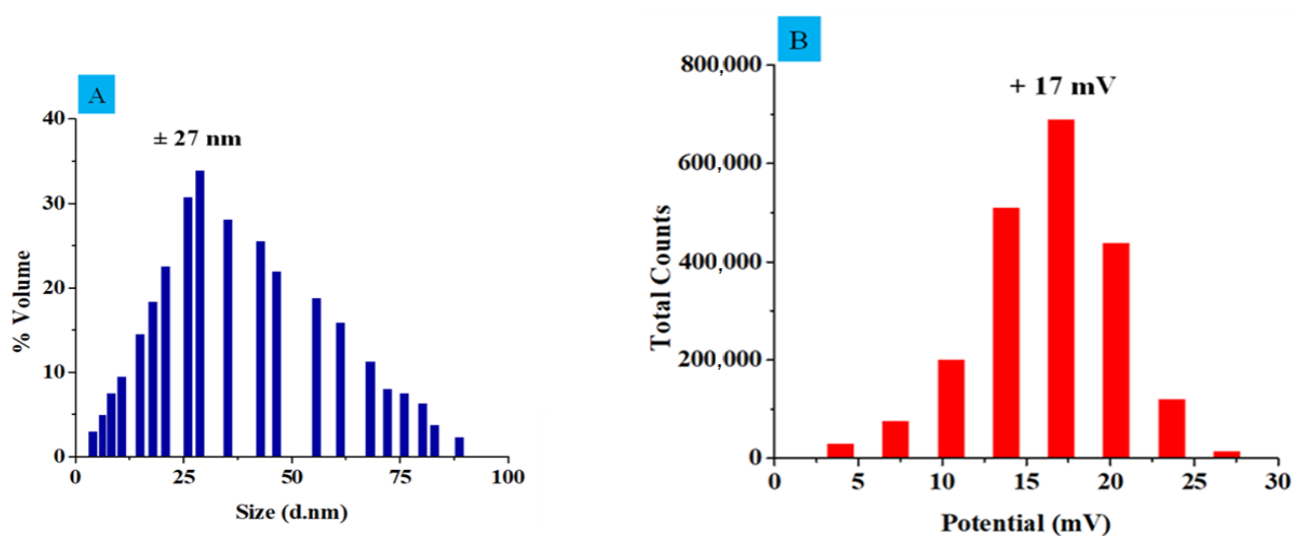


Figure 4. (A) Size of ZnO nanostructures around 27 nm. (B) Potential of ZnO nanostructures with about 17 ± 3 mV.

3.1.5. Analytical Performance of ZnO Nanostructures

The general properties of substances are significantly influenced by the sizes of the nanomaterials. As a result, semiconducting nanomaterials' size growth becomes crucial for examining the properties of the materials. It is common practice to use a UV–visible spectrometer to examine the absorption properties of nanocrystals [45,46]. For the continuous destruction of organic contaminants [47], namely, pentachlorophenol and trichlorophenol, the photocatalytic activity of a freshly synthesized ZnO nanoclump was examined. Some important processes, such as the use of sodium borohydride as a charged particle source, UV irradiation, and the dosage of the photocatalyst for the best percentage degradation, were tuned to manage the effectiveness of the nanocatalyst. Using a UV–visible spectrophotometer, the deterioration was seen. The strength of the absorption gradually decreased up to 90% during the degradation phase.

By using sodium borohydride (NaBH₄) as an instantaneous charged particle source as well as other supporting conditions, the predicted nanocatalyst's effectiveness was initially assessed to validate its relevance. The suggested nanocatalyst's capacity to degrade materials is considerably aided by sodium borohydride, an essential component [48]. The causes of the neutron derived from NaBH₄ and its supporting characteristics were looked into to analyze the effectiveness of the suggested nanocatalyst. The first step was to investigate the effects of variations in NaBH₄ concentration on the degradation, and it was discovered that there were substantial differences in peak intensities and the trend was declining. Reported declines of roughly 28% and 23% for PCP and TCP, respectively, were noted. This degradation rate is almost equal for both cases. The possible reason could be their response to UV light in the presence of NaBH₄. Figure 5A–C illustrate the absorption spectra of PCP, TCP, and the mixture of PCP and TCP, whereas Figure 5C demonstrates the mechanism of pollutant degradation that was calculated from Figure 5A–C. The absorption spectra show a continuous declining pattern, which was between 20 and 28. Figure 5D shows the percentage of deterioration, even though there was only a slight deterioration recorded after adding additional NaBH₄, and no significant drop in absorption coefficient was noticed. Additionally, it was noted that an extensive dosage of NaBH₄ was unable to offer a suitable solution due to the particular restrictions that may have resulted from the lack of any assistance in the collection or adsorption of hydride ions [49,50]. Later, this issue was overcome by the inclusion of a surface-enhanced ZnO nanostructure, which served as a firm foundation for the extraordinary hydride ion adsorption that significantly decreased the PCP and TCP molecules.

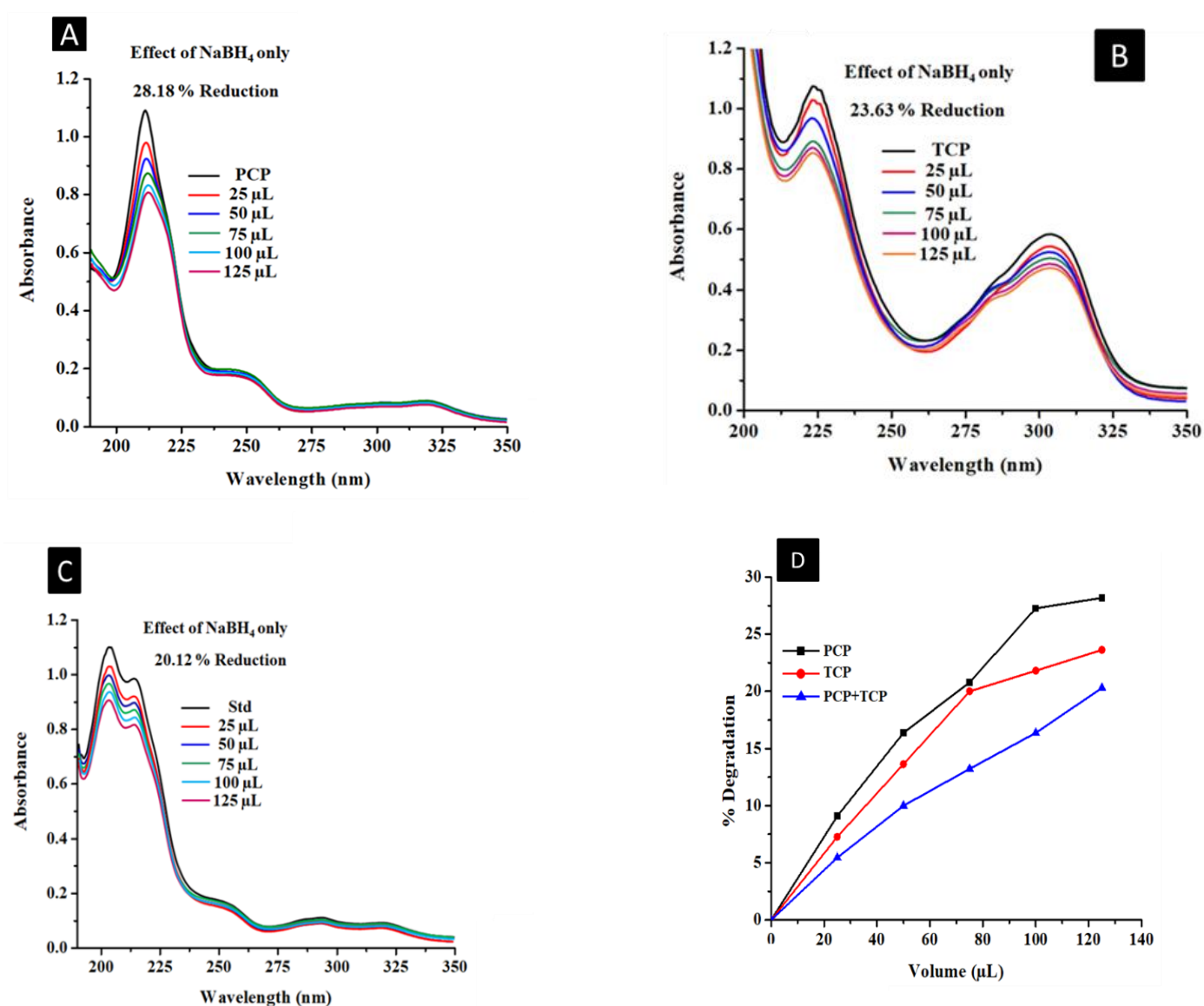


Figure 5. Absorption spectra of PCP and TCP individually (A,B) and simultaneously (C) with inset showing % degradation graph (D) in the absence of a catalyst using 25–125 µL NaBH₄ (0.005 M).

In addition to sodium borohydride (proton source) optimization, the sunlight effect appeared both separately and concurrently. For PCP and TCP, a discernible fluctuation in peak intensity was found during the usual period. As a result, 125 L of sodium borohydride was collected in quartz cells, and interacted for 1 h outside before spectra were eventually recorded. According to Figure 6A–C, there were deteriorations of about 34.45%, 32.33%, and 29.12%, respectively. However, no appreciable change was noticed when the solution was exposed to more sunshine radiation; just 1–2% was analyzed. Figure 6D shows the percentage of deterioration more clearly. Furthermore, it was unable to offer better results with a prolonged time of exposure because it was devoid of any means of capturing hydride ions. The issue was then resolved by the addition of ZnO nanostructures, which proved successful and offered sturdy support for the impressive adsorption of hydride ions that greatly reduced PCP and TCP [50]. Applying a reducing agent will increase deterioration and shorten the time it takes to complete the task, making it more effective and adequate.

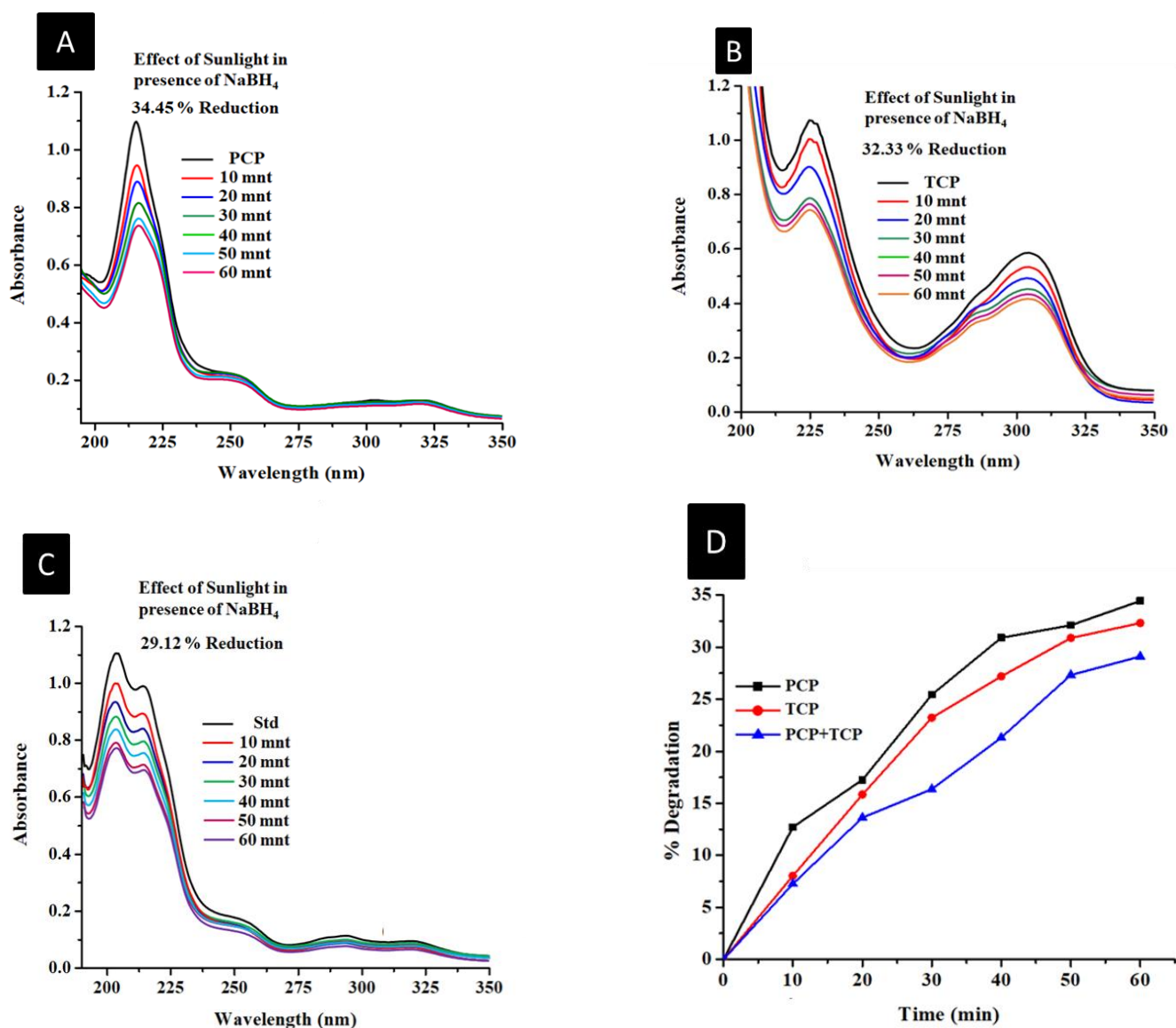


Figure 6. Absorption spectra of PCP and TCP individually and simultaneously (A–C) with inset showing % reduction graph (D) in the absence of a catalyst using 125 μL NaBH_4 (0.005 M) and exposure to sunlight for 10–60 min.

After adjusting the sodium borohydride and sunlight, the catalytic dosage coupled with the immediate proton must be maximized to determine the catalytic efficacy of the manufactured nanocatalyst. A test tube containing the appropriate amounts of PCP and TCP, and 125 L of NaBH_4 was used to assess this stage. After 3 min in the sunshine, spectra were collected. For all individual and concurrent studies, the catalytic readings were kept within a target band of 250 g. It was discovered that the peak intensities of PCP and TCP were significantly effective. Figure 7A–C illustrate the estimated 90%, 86%, and 85% deteriorations that were experienced, and Figure 7D also displays a more precise degree of deterioration [51]. The development of sodium borohydride protons (H^+), which are typically attached to the surfaces of nanomaterials, may be the reason for the increase in PCP and TCP degradation, thus enhancing the nanocatalyst activity. The catalytic regions on the zinc oxide surface expanded as the dose increased, speeding up the chemical reaction towards degradation [50,52].

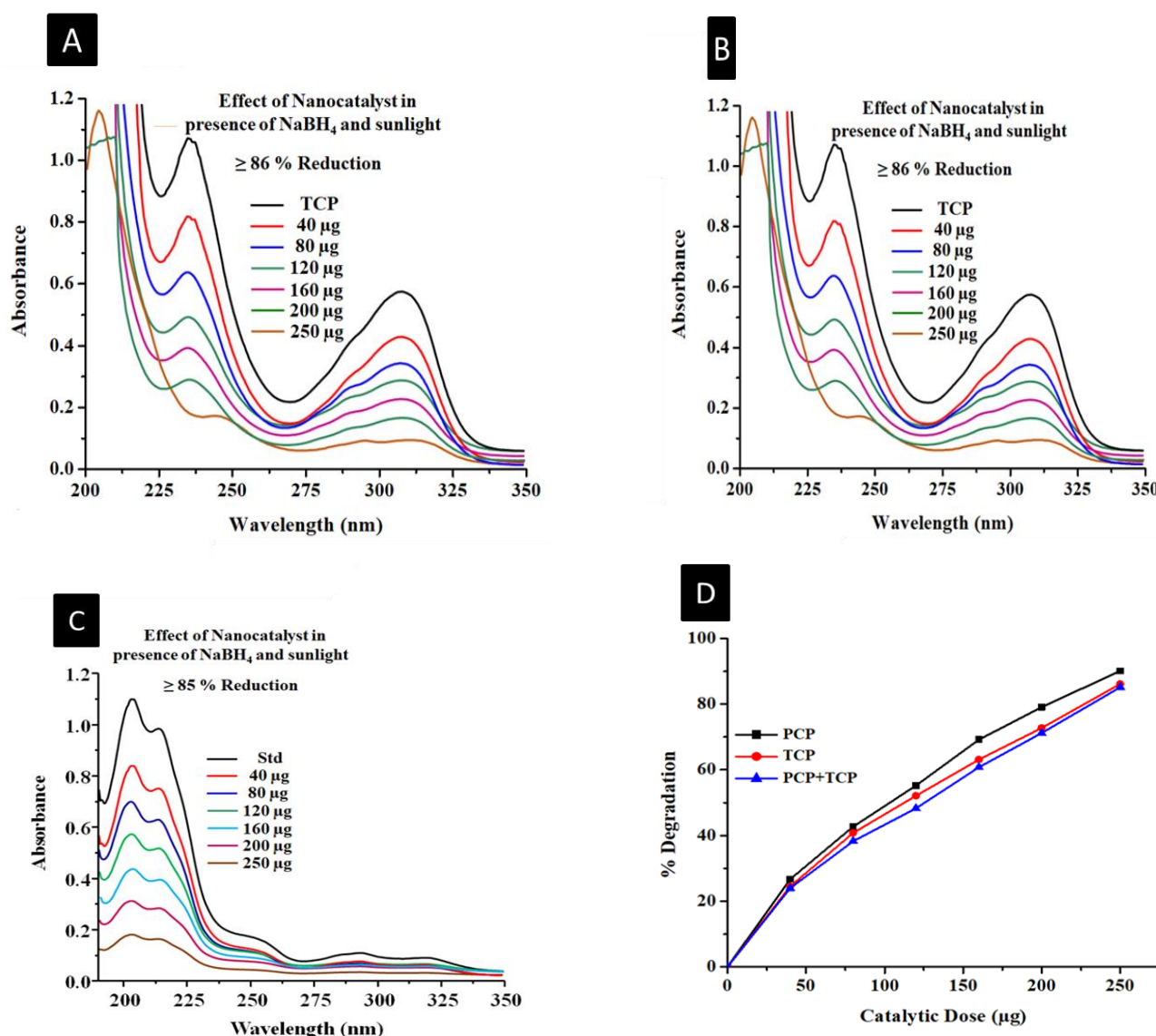


Figure 7. Absorption spectra of PCP and TCP separately and together (A–C) using 250 g of each substance, with an inset displaying a graph of the percentage of decrease (D) in the presence of 125 µL of NaBH₄ (0.005 M) and sunlight for 180 s.

3.1.6. Degradation Mechanism

As ZnO nanoparticles interact with solar light to form a mechanical effect, a void is continuously created in the photogenerated surface and a particle is excited to the bandgap from the conductive band (shown in Figure 8). It is possible to recombine or interact independently with these solar-produced holes' pairs of electrons. While oxygen deposited on the surface of the catalyst helps with building oxidant reactive protons, the holes it produces can interact and form OH radicals. In the end, an oxidized product was produced by subjecting the expected impurity to hydroxyl radical treatment (a strong oxidizing agent) [45]. Below is a summary of the entire sequential mechanism:



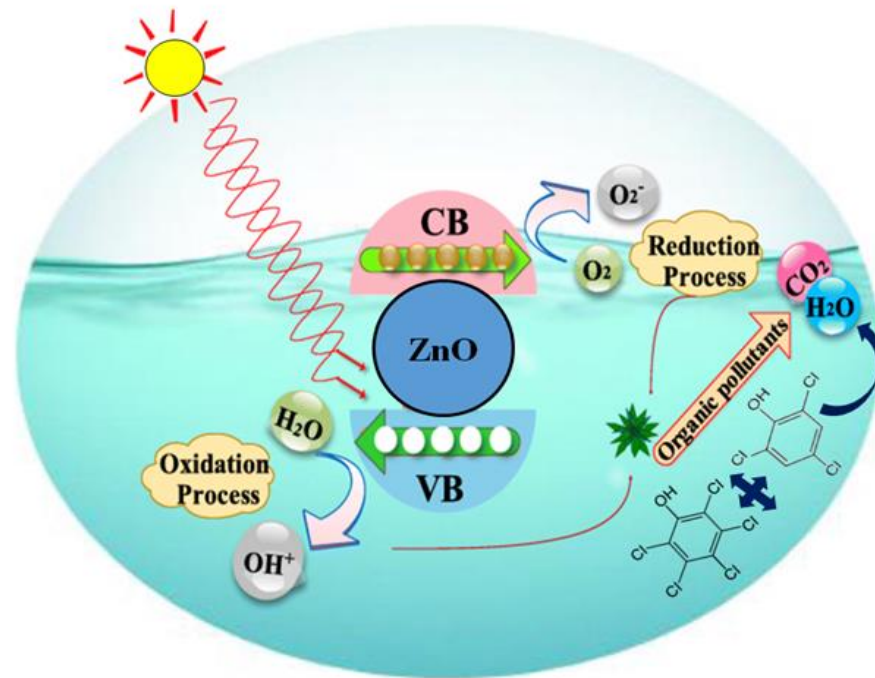


Figure 8. PCP and TCP degradation mechanism by zinc oxide nanostructures in the presence of sunlight.

4. Conclusions

In this research, ZnO nanoparticles were synthesized through the aqueous chemical growth method. Advanced characterization techniques such as SEM, XRD, EDS, FTIR, ZS, and ZP were used to characterize the ZnO nanostructures. When the materials were examined using XRD, the hexagonal wurtzite phase of ZnO was discovered. The photocatalytic degradation of chlorophenols chemicals in the environment shows that ZnO has a lot of potential, as it effectively played a key role in the degradation of chlorophenols. In the present study, well-organized ZnO nanostructures were used to degrade PCP and TCP in aqueous conditions. ZnO nanoparticles exposed to sunlight and sodium borohydride were effective in removing toxicity from chlorophenol-polluted water. The ZnO nanostructure was highly accountable for the exceptional photocatalytic degradation of PCP and TCP, displaying 85–90% in the presence of sunlight for 3 min in combination with a NaBH₄ nanocatalyst. The proposed nanocatalyst exhibited intense recyclability with an insignificant degradation efficiency. This work is very much suitable for industries that generate enormous amounts of polluted water, especially textile industries. This method of pollutant degradation is very much suited to this, as the degradation time is very short i.e., 3 min. The industries can re-use the water for various purposes, and can not only save their investments, but energy as well.

Author Contributions: Conceptualization, I.A.C. (Iftikhar Ahmed Channa) and A.D.C.; methodology A.H.P., I.A.C. (Imran Ali Chandio) and J.A.B.; writing, A.H.P., I.A.C. (Iftikhar Ahmed Channa) and J.A.; validation, I.A.C. (Iftikhar Ahmed Channa), A.D.C. and A.A.S.; investigation, J.A., I.A.C. (Imran Ali Chandio) and A.A.S.; supervision, A.D.C. and I.A.C. (Iftikhar Ahmed Channa); funding acquisition, S.J.G., M.N.B.J. All authors have read and agreed to the published version of the manuscript.

Funding: This research project was funded by Princess Nourah bint Abdulrahman University, Researchers Supporting Project number (PNURSP2022R108), Princess Nourah bint Abdulrahman University, Riyadh, Saudi Arabia.

Institutional Review Board Statement: Not Applicable.

Informed Consent Statement: Not Applicable.

Data Availability Statement: Data are available upon request from the corresponding authors.

Acknowledgments: This research project is supported by Princess Nourah Bint Abdulrahman University Researchers Supporting Project number (PNURSP2022R108), Princess Nourah Bint Abdulrahman University, Riyadh, Saudi Arabia.

Conflicts of Interest: The authors declare that they have no known competing financial interests or personal relationships that could have appeared to influence the work reported in this paper.

References

1. Leone, J.R.N.; Marta, F.D. Perception of Climate Change Effects over Time and the Contribution of Different Areas of Knowledge to Its Understanding and Mitigation. *Climate* **2022**, *10*, 7. [CrossRef]
2. Batool, S.A.; Liaquat, U.; Channa, I.A.; Gilani, S.J.; Makhdoom, M.A.; Yasir, M.; Ashfaq, J.; Jumah, M.N.B.; Rehman, M.A.U. Development and Characterization of Zein/Ag-Sr Doped Mesoporous Bioactive Glass Nanoparticles Coatings for Biomedical Applications. *Bioengineering* **2022**, *9*, 367. [CrossRef] [PubMed]
3. Ashfaq, J.; Channa, I.A.; Shaikh, A.A.; Chandio, A.D.; Shah, A.A.; Bughio, B.; Birmahani, A.; Alshehri, S.; Ghoneim, M.M. Gelatin- and Papaya-Based Biodegradable and Edible Packaging Films to Counter Plastic Waste Generation. *Materials* **2022**, *15*, 1046. [CrossRef] [PubMed]
4. Chakraborti, L.; Shimshack, J.P. Environmental disparities in urban Mexico: Evidence from toxic water pollution. *Resour. Energy Econ.* **2022**, *67*, 101281. [CrossRef]
5. Abro, S.H.; Chandio, A.; Channa, I.A.; Alaboodi, A.S. Design, Development and Characterization of Graphene Sand Nano-Composite for Water Filtration. *Pak. J. Sci. Ind. Res. Ser. A Phys. Sci.* **2020**, *63*, 118–122. [CrossRef]
6. Zhou, T.; Wang, Y.; Li, T.; Li, H.; Yang, C.; Sun, D.; Wang, D.; Liu, C.; Che, G. Fabricating magnetic hydrophilic molecularly imprinted resin with enhanced adsorption and recognition performance for targeted detecting chlorophenols in environmental water. *Chem. Eng. J.* **2021**, *420*, 129904. [CrossRef]
7. Igbinosa, E.O.; Odjadjare, E.E.; Chigor, V.N.; Igbinosa, I.H.; Emoghene, A.O.; Ekhaize, F.O.; Igiehon, N.O.; Idemudia, O.G. Toxicological Profile of Chlorophenols and Their Derivatives in the Environment: The Public Health Perspective. *Sci. World J.* **2013**, *2013*, 460215. [CrossRef]
8. Enyoh, C.E.; Isiuku, B.O. Competitive biosorption and phytotoxicity of chlorophenols in aqueous solution to *Canna indica* L. *Curr. Res. Green Sustain. Chem.* **2021**, *4*, 100094. [CrossRef]
9. Dai, M.; Rogers, J.B.; Warner, J.R.; Copley, S.D. A Previously Unrecognized Step in Pentachlorophenol Degradation in *Sphingobium chlorophenolicum* Is Catalyzed by Tetrachlorobenzoquinone Reductase (PcpD). *J. Bacteriology* **2003**, *185*, 302–310. [CrossRef]
10. Hunge, Y.; Yadav, A.; Kang, S.-W.; Kim, H. Facile synthesis of multitasking composite of Silver nanoparticle with Zinc oxide for 4-nitrophenol reduction, photocatalytic hydrogen production, and 4-chlorophenol degradation. *J. Alloys Compd.* **2022**, *928*, 167133. [CrossRef]
11. Georgekutty, R.; Seery, M.K.; Pillai, S.C. A Highly Efficient Ag-ZnO Photocatalyst: Synthesis, Properties, and Mechanism. *J. Phys. Chem. C* **2008**, *112*, 13563–13570. [CrossRef]
12. Dieter, L.; Horwitz, C.P.; Collins, T.J. Rapid Total Destruction of Chlorophenols by Activated Hydrogen Peroxide. *Science* **2002**. [CrossRef]
13. Sriram, G.; Bendre, A.; Mariappan, E.; Altalhi, T.; Kigga, M.; Ching, Y.C.; Jung, H.-Y.; Bhaduri, B.; Kurkuri, M. Recent trends in the application of metal-organic frameworks (MOFs) for the removal of toxic dyes and their removal mechanism—A review. *Sustain. Mater. Technol.* **2022**, *31*, e00378. [CrossRef]
14. Khan, I.; Yuan, A.; Khan, A.; Khan, S.; Khan, S.; Shah, S.A.; Yaseen, W.; Cui, Y.; Shen, X.; Wang, X. Efficient Visible-Light Activities of TiO₂ decorated and Cr³⁺ incorporated-porous SmFeO₃ for CO₂ conversion and 4-chlorophenol degradation. *Surf. Interfaces* **2022**, *34*, 102358. [CrossRef]
15. Samuchiwal, S.; Bhattacharya, A.; Malik, A. Treatment of textile effluent using an anaerobic reactor integrated with activated carbon and ultrafiltration unit (AN-ACF-UF process) targeting salt recovery and its reusability potential in the pad-batch process. *J. Water Process Eng.* **2021**, *40*, 101770. [CrossRef]
16. Channa, I.A.; Ashfaq, J.; Gilani, S.J.; Shah, A.A.; Chandio, A.D.; Jumah, M.N.B. UV Blocking and Oxygen Barrier Coatings Based on Polyvinyl Alcohol and Zinc Oxide Nanoparticles for Packaging Applications. *Coatings* **2022**, *12*, 897. [CrossRef]
17. Sajid, M. Nanomaterials: Types, properties, recent advances, and toxicity concerns. *Curr. Opin. Environ. Sci. Health* **2021**, *25*, 100319. [CrossRef]
18. Biener, J.; Wittstock, A.; Baumann, T.F.; Weissmüller, J.; Bäumer, M.; Hamza, A.V. Surface Chemistry in Nanoscale Materials. *Materials* **2009**, *2*, 2404–2428. [CrossRef]
19. Antonopoulou, M.; Kosma, C.; Albanis, T.; Konstantinou, I. An overview of homogeneous and heterogeneous photocatalysis applications for the removal of pharmaceutical compounds from real or synthetic hospital wastewaters under lab or pilot scale. *Sci. Total Environ.* **2021**, *765*, 144163. [CrossRef]

20. Ba-Abbad, M.M.; Takriff, M.S.; Said, M.; Benamor, A.; Nasser, M.S.; Mohammad, A.W. Photocatalytic Degradation of Pentachlorophenol Using ZnO Nanoparticles: Study of Intermediates and Toxicity. *Int. J. Environ. Res.* **2017**, *11*, 461–473. [[CrossRef](#)]
21. Atwan, A.A.; Elmehasseb, I.M.; Talha, N.; El-Kemary, M. Parameters affecting carbofuran photocatalytic degradation in water using ZnO nanoparticles. *J. Chin. Chem. Soc.* **2020**, *67*, 1833–1842. [[CrossRef](#)]
22. Ullah, I.; Siddiqui, M.A.; Liu, H.; Kolawole, S.K.; Zhang, J.; Zhang, S.; Ren, L.; Yang, K. Mechanical, Biological, and Antibacterial Characteristics of Plasma-Sprayed (Sr,Zn) Substituted Hydroxyapatite Coating. *ACS Biomater. Sci. Eng.* **2020**, *6*, 1355–1366. [[CrossRef](#)] [[PubMed](#)]
23. Ujjan, Z.A.; Bhatti, M.A.; Shah, A.A.; Tahira, A.; Shaikh, N.M.; Kumar, S.; Mugheri, A.Q.; Medany, S.S.; Nafady, A.; Alnjiman, F.; et al. Simultaneous doping of sulfur and chloride ions into ZnO nanorods for improved photocatalytic properties towards degradation of methylene blue. *Ceram. Int.* **2022**, *48*, 5535–5545. [[CrossRef](#)]
24. Kumar, P.S.; Maniam, S.; Sundaramurthy, J.; Arokiaraj, J.; Mangalaraj, D.; Rajarathnam, D.; Srinivasan, M.; Jian, L. Growth specificity of vertical ZnO nanorods on patterned seeded substrates through integrated chemical process. *Mater. Chem. Phys.* **2012**, *133*, 126–134. [[CrossRef](#)]
25. Amiruddin, R.; Kumar, M.S. Enhanced visible emission from vertically aligned ZnO nanostructures by aqueous chemical growth process. *J. Lumin.* **2014**, *155*, 149–155. [[CrossRef](#)]
26. Rajivgandhi, G.; Gnanamangai, B.M.; Prabha, T.H.; Poornima, S.; Maruthupandy, M.; Alharbi, N.S.; Kadaikunnan, S.; Li, W.-J. Biosynthesized zinc oxide nanoparticles (ZnO NPs) using actinomycetes enhance the anti-bacterial efficacy against *K. Pneumoniae*. *J. King Saud Univ. Sci.* **2022**, *34*, 101731. [[CrossRef](#)]
27. Malakootian, M.; Khatami, M.; Mahdizadeh, H.; Nasiri, A.; Gharaghani, M.A. A study on the photocatalytic degradation of p-Nitroaniline on glass plates by Thermo-Immobilized ZnO nanoparticle. *Inorg. Nano-Metal Chem.* **2020**, *50*, 124–135. [[CrossRef](#)]
28. Zyoud, A.H.; Asaad, S.; Zyoud, S.H.; Zyoud, S.H.; Helal, M.H.; Qamhieh, N.; Hajamohideen, A.; Hilal, H.S. Raw clay supported ZnO nanoparticles in photodegradation of 2-chlorophenol under direct solar radiations. *J. Environ. Chem. Eng.* **2020**, *8*, 104227. [[CrossRef](#)]
29. Ben Ali, M.; Barras, A.; Addad, A.; Sieber, B.; Elhouichet, H.; Férid, M.; Szunerits, S.; Boukherroub, R. Co₂SnO₄ nanoparticles as a high performance catalyst for oxidative degradation of rhodamine B dye and pentachlorophenol by activation of peroxymonosulfate. *Phys. Chem. Chem. Phys.* **2017**, *19*, 6569–6578. [[CrossRef](#)]
30. Zhang, J.; Chen, Z.; Guo, R.; Shan, D.; Zhao, Y.; Linghu, X.; Shu, Y.; Wang, B. Synthesis of nano-sized Ag₃PW₁₂O₄₀/ZnO heterojunction as a photocatalyst for degradation of organic pollutants under simulated sunlight. *Arab. J. Chem.* **2022**, *15*, 103659. [[CrossRef](#)]
31. Mahdavi, K.; Salavati-Niasari, M.; Amiri, O.; Ghanbari, M. Synthesis of La₉33Si₆O₂₆ nano-photocatalysts by ultrasonically accelerated method for comparing water treatment efficiency with changing conditions. *Arab. J. Chem.* **2022**, *15*, 103481. [[CrossRef](#)]
32. Siddiqui, M.A.; Ren, L.; Macdonald, D.D.; Yang, K. Effect of Cu on the passivity of Ti-xCu (x = 0, 3 and 5 wt%) alloy in phosphate-buffered saline solution within the framework of PDM-II. *Electrochim. Acta* **2021**, *386*, 138466. [[CrossRef](#)]
33. Xin, M. Crystal Structure and Optical Properties of ZnO:Ce Nano Film. *Molecules* **2022**, *27*, 5308. [[CrossRef](#)] [[PubMed](#)]
34. Dinesh, V.P.; Biji, P.; Ashok, A.; Dhara, S.K.; Kamruddin, M.; Tyagi, A.K.; Raj, B. Plasmon-mediated, highly enhanced photocatalytic degradation of industrial textile dyes using hybrid ZnO@Ag core-shell nanorods. *RSC Adv.* **2014**, *4*, 58930–58940. [[CrossRef](#)]
35. De Lucas-Gil, E.; Menéndez, J.; Pascual, L.; Fernández, J.F.; Rubio-Marcos, F. The Benefits of the ZnO/Clay Composite Formation as a Promising Antifungal Coating for Paint Applications. *Appl. Sci.* **2020**, *10*, 1322. [[CrossRef](#)]
36. Wahyuono, R.A.; Schmidt, C.; Dellith, A.; Dellith, J.; Schulz, M.; Seyring, M.; Rettenmayr, M.; Plentz, J.; Dietzek, B. ZnO nanoflowers-based photoanodes: Aqueous chemical synthesis, microstructure and optical properties. *Open Chem.* **2016**, *14*, 158–169. [[CrossRef](#)]
37. Liu, J.; Wu, W.; Bai, S.; Qin, Y. Synthesis of High Crystallinity ZnO Nanowire Array on Polymer Substrate and Flexible Fiber-Based Sensor. *ACS Appl. Mater. Interfaces* **2011**, *3*, 4197–4200. [[CrossRef](#)]
38. Jain, D.; Shivani; Bhojiya, A.A.; Singh, H.; Daima, H.K.; Singh, M.; Mohanty, S.R.; Stephen, B.J.; Singh, A. Microbial Fabrication of Zinc Oxide Nanoparticles and Evaluation of Their Antimicrobial and Photocatalytic Properties. *Front. Chem.* **2020**, *8*, 778. [[CrossRef](#)]
39. Fecete, I.; Vadrine, J.C. Nanoporous Materials as New Engineered Catalysts for the Synthesis of Green Fuels. *Molecules* **2015**, *20*, 5638–5666. [[CrossRef](#)]
40. Muhammad, W.; Ullah, N.; Haroon, M.; Abbasi, B.H. Optical, morphological and biological analysis of zinc oxide nanoparticles (ZnO NPs) using *Papaver somniferum* L. *RSC Adv.* **2019**, *9*, 29541–29548. [[CrossRef](#)]
41. Jan, H.; Shah, M.; Usman, H.; Khan, M.A.; Zia, M.; Hano, C.; Abbasi, B.H. Biogenic Synthesis and Characterization of Antimicrobial and Antiparasitic Zinc Oxide (ZnO) Nanoparticles Using Aqueous Extracts of the Himalayan Columbine (*Aquilegia pubiflora*). *Front. Mater.* **2020**, *7*, 249. [[CrossRef](#)]
42. Jayarambabu, N.; Kumari, B.S.; Rao, K.V.; Prabhu, Y.T. Germination and growth characteristics of mungbean seeds (*Vigna radiata* L.) affected by synthesized zinc oxide nanoparticles. *Int. J. Curr. Eng. Technol.* **2014**, *4*, 2347–5161.
43. Astruc, D. Introduction: Nanoparticles in Catalysis. *Chem. Rev.* **2020**, *120*, 461–463. [[CrossRef](#)] [[PubMed](#)]
44. Akbar, N.; Aslam, Z.; Siddiqui, R.; Shah, M.R.; Khan, N.A. Zinc oxide nanoparticles conjugated with clinically-approved medicines as potential antibacterial molecules. *AMB Express* **2021**, *11*, 104. [[CrossRef](#)]

45. Wang, Y.; Yang, C.; Liu, Y.; Fan, Y.; Dang, F.; Qiu, Y.; Zhou, H.; Wang, W.; Liu, Y. Solvothermal Synthesis of ZnO Nanoparticles for Photocatalytic Degradation of Methyl Orange and p-Nitrophenol. *Water* **2021**, *13*, 3224. [[CrossRef](#)]
46. Talam, S.; Karumuri, S.R.; Gunnam, N. Synthesis, Characterization, and Spectroscopic Properties of ZnO Nanoparticles. *Int. Sch. Res. Not. Nanotechnol.* **2012**, *2012*, 372505. [[CrossRef](#)]
47. Channa, I.A.; Distler, A.; Brabec, C.J.; Egelhaaf, H.-J. 9—Solution-coated barriers for organic electronics. In *Organic Flexible Electronics: Fundamentals, Devices, and Applications*; Cosseddu, P., Caironi, M., Eds.; Woodhead Publishing Series in Electronic and Optical, Materials; Woodhead Publishing: Sawston, UK, 2021; pp. 249–303. [[CrossRef](#)]
48. Siddiqui, M.A.; Ullah, I.; Liu, H.; Zhang, S.; Ren, L.; Yang, K. Preliminary study of adsorption behavior of bovine serum albumin (BSA) protein and its effect on antibacterial and corrosion property of Ti-3Cu alloy. *J. Mater. Sci. Technol.* **2021**, *80*, 117–127. [[CrossRef](#)]
49. Siddiqui, M.A.; Ullah, I.; Kolawole, S.K.; Peng, C.; Wang, J.; Ren, L.; Yang, K.; Macdonald, D.D. Study the existing form of copper (p-type oxide/segregation) and its release mechanism from the passive film of Ti-7Cu alloy. *Corros. Sci.* **2021**, *190*, 109693. [[CrossRef](#)]
50. Mahar, Z.A.; Shar, G.Q.; Balouch, A. Fabrication of ZnO nanocatalyst as an excellent heterogeneous catalyst applicant for Methyl Orange dye degradation in aqueous medium. *Res. Sq.* **2021**. [[CrossRef](#)]
51. Bhatti, M.A.; Shah, A.A.; Almani, K.F.; Tahira, A.; Chalangar, S.E.; Chandio, A.D.; Nur, O.; Willander, M.; Ibupoto, Z.H. Efficient photo catalysts based on silver doped ZnO nanorods for the photo degradation of methyl orange. *Ceram. Int.* **2019**, *45*, 23289–23297. [[CrossRef](#)]
52. Shah, A.A.; Bhatti, M.A.; Tahira, A.; Chandio, A.D.; Channa, I.A.; Sahito, A.G.; Chalangar, E.; Willander, M.; Nur, O.; Ibupoto, Z.H. Facile synthesis of copper doped ZnO nanorods for the efficient photo degradation of methylene blue and methyl orange. *Ceram. Int.* **2020**, *46*, 9997–10005. [[CrossRef](#)]